Graphical Table of Content

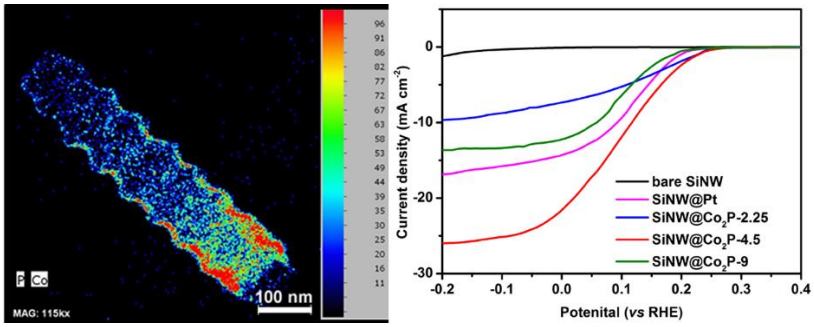

Di-cobalt phosphide (Co_2P) has been conformally and continuously deposited on the surface of silicon nanowire (SiNW) arrays via a simple and cost-effective approach, which offers dual functions as both a passivation layer to protect silicon from corrosion and a catalyst layer promoting the hydrogen evolution reaction. The as-fabricated SiNW@Co_2P core/shell photocathode shows excellent photoelectrocatalytic hydrogen evolution performance.

Conformal and continuous deposition of bifunctional cobalt phosphide layers on p-silicon nanowire arrays for improved solar hydrogen evolution

Sitaramanjaneva Mouli Thalluri[1], Jerome Borme[1], Kang Yu[1,2], Junyuan Xu[1], Isilda Amorim[1], Joao Gaspar[1], Liang Qiao[3], Paulo Ferreira[1,2], Pedro Alpuim[1,4], and Lifeng Liu[1,*]

[1] International Iberian Nanotechnology Laboratory (INL), Av. Mestre. Jose Veiga, 4715-330 Braga, Portugal

[2] Materials Science and Engineering Program, University of Texas at Austin, Austin, TX78712, USA

[3] Department of Chemistry, State Key Laboratory of Molecular Engineering of Polymers and Institute of Biomedical Sciences, Fudan University, Shanghai 200433, P. R. China

[4] Center of Physics, University of Minho, 4710-057 Braga, Portugal

* Address correspondence to lifeng.liu@inl.int

Abstract

p-Silicon nanowire (SiNW) arrays have been extensively investigated in recent years as promising photocathodes for solar-driven hydrogen evolution. However, it remains challenging to fabricate SiNW photocathodes having both high photoelectrocatalytic activity and long-term operational stability through a simple and affordable approach. Herein, we report conformal and continuous deposition of a di-cobalt phosphide (Co_2P) layer on lithography-patterned highly-ordered SiNW arrays *via* a cost-effective drop-casting method followed by a low-temperature phosphorization treatment. The as-deposited Co_2P layer consists of crystalline nanoparticles and has an intimate contact with silicon nanowires, forming a well-defined SiNW@Co_2P core/shell nanostructure. The conformal and continuous Co_2P layer endows dual functions: on the one hand, it serves as a highly-efficient catalyst capable of substantially improving the photoelectrocatalytic activity towards the hydrogen evolution reaction (HER); on the other hand, it can effectively passivate SiNWs to protect them from photo-oxidation, thus prolonging the lifetime of the electrode. As a consequence, when used for solar-driven hydrogen evolution, the SiNW@Co_2P photocathode with an optimized Co_2P layer thickness exhibits a high photocurrent density of -21.9 mA cm^{-2} and excellent operational stability of up to 20 hours, outperforming many nanostructured silicon photocathodes reported in the literature. The combination of passivation and catalytic functions in a single continuous layer represents a promising strategy for designing high-performance semiconductor photoelectrodes for use in solar-driven water splitting, which may simplify the fabrication procedures and potentially reduce the production cost.

Keywords:

solar-driven hydrogen evolution, silicon nanowire, cobalt phosphide, photoelectrochemical water splitting, drop-casting

1. Introduction

The ever-growing global population has raised huge demand for energy. In order to avoid the depletion of non-renewable fossil fuels and to alleviate the serious environmental pollution associated with the consumption of fossil fuels, a consensus has been reached that renewable energies should be deployed on a large scale and steadily replace fossil fuels until they dominate the global energy supply [1]. Converting solar energy into storable and clean chemical fuels such as hydrogen (H_2) through photoelectrochemical (PEC) water splitting represents a promising and sustainable approach to solar energy utilization and storage, and has re-gained considerable research interest in recent years [2-5]. To make the PEC-derived H_2 economically competitive and affordable, low-cost, earth-abundant yet highly-efficient semiconductors and electrocatalysts must be used. To this end, silicon (Si) stands out among many other semiconductor materials because it is the second most abundant element in the crust and inexpensive in price; it has a band gap (1.1 eV) allowing for light absorption over a wide window of the solar spectrum, and its conduction band edge is positioned negatively relative to the proton reduction potential, which is the right position for charge transfer when driving the hydrogen evolution reaction (HER) [6, 7]; moreover, the processing techniques of Si are well established and can be readily used in photoelectrode development. In terms of electrocatalysts, platinum (Pt) has been the state-of-the-art for the HER. However, the prohibitive cost and scarcity of Pt are the major limiting factors for large-scale applications of this efficient catalyst. In this context, many research works have recently focused on non-precious transition metal based HER catalysts including chalcogenides [8-15], phosphides [16-24], carbides [25-27], borides [28, 29] and nitrides [30], and HER performance favorably comparable to that of Pt was already reported.

In the last few years, unremitting efforts have been made to improve the PEC performance of Si based photocathodes by either nanostructuring Si or coupling efficient HER catalysts with Si or the combination of both strategies [8, 31-36]. However, in many cases the catalysts only sparsely cover the surface of Si micro-/nano-structured photoelectrodes [18, 19, 37-40], and the Si exposed to aqueous electrolyte will get oxidized over time, eventually leading to device failure. This has posed a great challenge for practical use of Si-based photoelectrodes in solar-driven H_2 evolution. To overcome this problem, a chemically inert passivation layer (e.g. TiO_2) was introduced to prevent the formation of a silicon oxide insulating layer on Si, followed by coupling of HER catalysts on the deposited passivation layer [31, 37, 41-43]. This Si/passivation layer/catalyst configuration has been demonstrated to be able to substantially improve the lifetime of Si-based photoelectrodes, but nevertheless the photocurrent generated will in many cases be compromised due to the loss of electrons when tunneling across the passivation layer [44].

Herein, we report conformal and continuous deposition of a di-cobalt phosphide (Co_2P) layer on highly-ordered Si nanowire (SiNW) arrays using a simple and cost-effective drop-casting method, followed by a post-phosphorization treatment. This single Co_2P layer affords dual functions: on the one hand, it can efficiently catalyze the HER given its high electrocatalytic activity that has been extensively demonstrated recently [18, 20, 23, 45, 46]; on the other hand, it serves as an effective passivation layer protecting SiNWs from photo-oxidation over long-term operation. The as-fabricated SiNW@Co_2P core/shell photocathodes exhibit a high photocurrent density of -21.9 mA cm^{-2} at 0 V *vs* reversible hydrogen electrode (RHE) in 0.5 M H_2SO_4, and can sustain under PEC operation conditions for at least 20 h without obvious degradation.

2. Results and Discussion

The SiNWs were fabricated by standard e-beam lithography and subsequent deep reactive ion etching (DRIE) processes, as described in Experimental Section. The as-fabricated SiNWs have a wavy side wall (**Figure 2a**), which resulted from the alternate passivation and etching steps during the DRIE process. Similar structural feature was also observed previously in Si microwires (SiMWs) fabricated by the top-down RIE process [8, 47]. To incorporate the Co_2P layer, a mixed solution of cobalt acetate and ethanol with different concentrations of Co^{2+} ranging from 2.25 to 62 mM was drop-cast on the surface of SiNW arrays, and was dried at ambient conditions. A phosphorization treatment was then performed in a tube furnace using red phosphorous as the source of phosphorous (see Experimental Section). All steps involved in the process of fabrication are schematically illustrated in **Figure 1**.

Figure 2b-2d show typical scanning electron microscopy (SEM) images of the resulting SiNW@Co_2P photoelectrodes prepared with Co^{2+} concentrations of 9, 18, and 36 mM (denoted as SiNW@Co_2P-X, X = 9, 18 and 36). No discernable difference is found between SiNW@Co_2P-X (X ≤9 mM) and the as-fabricated SiNW array, in appearance (**Figure S1**). However, as the Co^{2+} precursor concentration increases to 18 and 36 mM, the diameter of NWs becomes larger and some irregular particles are found to coat on the side walls of NWs (**Figure 2c** and **2d**). Moreover, it is observed that the parent Si substrate is also coated with a thick layer of Co_2P. In appearance, SiNW@Co_2P-18 and SiNW@Co_2P-36 are darker than SiNW@Co_2P-X (X ≤9 mM).

To gain further insight into the microstructure of the deposited Co_2P layer, transmission electron microscopy (TEM) observations were carried out. **Figure 3a** shows a montage TEM image of a single SiNW@Co_2P-9, where a layer of Co_2P is seen to continuously and conformally coat on the entire surface of the NW, forming a core/shell nanostructure. It is noted that the thickness of the Co_2P layer varies from top to bottom of the NW. This non-uniformity is believed

to result from the uneven distribution of the precursor solution during the drop-casting process, driven by the gravimetric effect. The non-uniform layer thickness can be resolved more clearly in the signal map of Co_2P along the NW, as shown in **Figure 3b**, where Co_2P is found to be more predominant around the root of the NW than on the top (see also energy-dispersive X-ray spectra, i.e. EDS in **Figure S2**). A closer look at the NW surface shows that the coating layer consists of many nanoparticles (**Figure 3c**). These nanoparticles (NPs) have typical diameters ranging from 3 to 6 nm and densely distribute on the surface of the NW. Selected-area electron diffraction (SAED) analysis of the NPs shows a well-defined ring pattern, which has been indexed as the orthorhombic phase of Co_2P (JCPDS No. 00-032-0306). High-resolution TEM (HRTEM) examination further confirmed the high degree of crystallinity of individual NPs. As shown in **Figure 3e**, the measured inter-planar distance of the NP is about 0.33 nm, corresponding to the lattice spacing of the (020) crystal planes of orthorhombic Co_2P.

To further investigate the distribution of Co_2P on the surface of SiNWs, elemental mapping was performed in high-angle annular dark-field scanning transmission electron microscopy (HAADF-STEM) mode. **Figure 4a** displays a representative HAADF-STEM image of SiNW@Co_2P where the particulate feature of Co_2P can be observed more clearly. As revealed by the elemental maps in **Figures 4b-4e**, both Co and P are continuously and conformally deposited on the surface of the SiNW, resulting in a core/shell structure, which agrees well with the bright-field TEM observation (**Figure 3a**). It is worth mentioning that conformal and continuous coatings of Co_2P were also observed for the photocathode of SiNW@Co_2P-4.5 (**Figure S3**), indicating that solution-based drop-casting is an effective way of coating nanostructured photoelectrodes with a thin conformal passivation/catalyst layer.

The PEC performance of SiNW@Co_2P photocathodes was comprehensively assessed in three-electrode configuration in 0.5 M H_2SO_4 (pH = 0.3) under 100 mW cm^{-2} illumination using linear scan voltammetry (LSV), Mott-Schottky (M-S) analysis, electrochemical impedance spectroscopy (EIS) and chronoamperometry (CA). For comparison, Pt NP decorated SiNW arrays (i.e. SiNW@Pt) were also fabricated and tested under the same conditions (see Experimental section for details). **Figure 5a** shows the LSV curves of bare SiNW, SiNW@Pt, and SiNW@Co_2P-X (X = 2.25, 4.5 and 9 mM) photocathodes on the reversible hydrogen electrode (RHE) scale. LSV curves of more SiNW@Co_2P-X samples are presented in **Figure S4**. The bare SiNW photocathode only generates negligible photocurrent at 0 V *vs* RHE (*ca.* -0.1 mA cm^{-2}), and shows an onset potential (U_{onset}, defined as the potential at which the cathodic photocurrent density is -0.5 mA cm^{-2}) of -0.14 V *vs* RHE. Upon coupling with the Co_2P catalyst, the onset potentials of SiNW@Co_2P-X photocathodes are significantly shifted towards the positive direction, reaching +0.24, +0.25 and +0.20 V *vs* RHE for SiNW@Co_2P-2.25, SiNW@Co_2P-4.5 and SiNW@Co_2P-9, respectively. Positive shift of the onset potential was repetitively reported previously when Si-based photocathodes were coupled with HER catalysts, which can be ascribed to the suppression of the recombination of photo-generated charge carriers [31]. Besides, the photocurrent density at 0 V *vs* RHE (J_0) of SiNW@Co_2P-X photocathodes is substantially enhanced, amounting to -7.4, -21.9 and -12.2 mA cm^{-2} for SiNW@Co_2P-2.25, SiNW@Co_2P-4.5 and SiNW@Co_2P-9, respectively. Among all samples investigated, SiNW@Co_2P-4.5 is the best-performing one: it is not only better than the SiNW@Pt control sample, which has U_{onset} of +0.21 V *vs* RHE and J_0 of -14.4 mA cm^{-2}, but also outperforms many Si-based photocathodes reported previously in the literature (**Table S1**) such as MoO_xS_y decorated SiMW arrays (U_{onset} = +0.24 V and J_0 = -9.83 mA cm^{-2}) [8], reduced graphene oxide-decorated SiNWs (U_{onset} = +0.206 V and J_0 = -3 mA cm^{-2}) [48], MoS_2-wrapped

SiNWs (U_{onset} = +0.3 V and J_0 = -15 mA cm^{-2}) [12], W_2C modified SiNWs (U_{onset} = +0.2 V and J_0 = -16 mA cm^{-2}) [27], and SiMW@cobalt dichalcogenide (U_{onset} = +0.29 V and J_0 = -3.22 mA cm^{-2}) [14]. SiNW@Co_2P photocathodes prepared with precursor concentrations higher than 9 mM were also tested (**Figure S4**), J_0 and the limiting photocurrent densities of these photocathodes are found to decrease as the precursor concentration increases. This might result from the increase in series resistance due to carrier depletion resulting from the reduced light absorption by the SiNW electrodes as a consequence of the increased thickness of the Co_2P layer.

Capacitance-voltage measurements were performed in the dark in 0.5 M H_2SO_4 at a frequency of 10 kHz to further investigate the flat band potential (U_{fb}) of the photocathodes. **Figure 5b** shows the M-S plots of the bare SiNW arrays and the best-performing SiNW@Co_2P-4.5 electrodes. Both SiNW and SiNW@Co_2P-4.5 show a negative M-S slope, characteristic of p-type semiconductors. U_{fb} can be derived from the following M-S equation [48]:

$$\frac{1}{C^2} = 2\frac{U_a - U_{fb} - \frac{kT}{q}}{qN_d\varepsilon_s\varepsilon_0 A^2} \quad (1)$$

where C is the space charge capacity, U_a stands for the applied potential, k represents the Boltzmann constant, T is the absolute temperature, q the electron charge, N_d the donor density, ε_s the dielectric constant of materials, ε_0 the electric permittivity of vacuum, and A the surface area. The band bending (U_b) of semiconductor photoelectrodes can be determined by the applied potential and U_{fb} through the following formula [48, 49]:

$$U_b = U_a - U_{fb} \quad (2)$$

Since U_a is negative under the cathodic reaction for proton reduction, a large U_{fb} will lead to a large absolute value of U_b, namely, a photocathode having a more positive U_{fb} will exhibit a larger band bending. As a result, the separation of photo-generated electrons and holes will proceed faster at the electrode/electrolyte interface, and meanwhile the surface charge trapping and

recombination can be largely suppressed. According to **Figure 5b**, U_{fb} of SiNW and SiNW@Co_2P-4.5 is +0.23 and +0.33 V *vs* RHE, respectively, suggesting that a larger band bending can be achieved for the SiNW@Co_2P-4.5 photocathode. This reasonably explains why remarkably large U_{onset} and J_0 were obtained for the SiNW@Co_2P photocathodes.

The charge transfer kinetics at the interface between the electrolyte and bare SiNW or SiNW@Co_2P-4.5 was further studied at +0.15 V *vs* RHE using EIS under 100 mW cm^{-2} illumination. **Figure 5c** shows the EIS Nyquist plots of the SiNW and SiNW@Co_2P-4.5 photocathodes. The Nyquist plots are fitted with the equivalent circuit models shown in the inset of **Figure 5c**, where R_s represents the equivalent series resistance, W_d is the Warburg resistance arising from diffusion in NW arrays, Q_1 and Q_2 are the constant phase elements, R_1 stands for the charge transport resistance at the interface between SiNW and Co_2P layer, and R_{ct} is the resistance of charge transfer at the electrode/electrolyte interface. As revealed in the zoomed view of Nyquist plots in **Figure 5c** inset, after coupling with the Co_2P layer, R_s of the SiNW@Co_2P-4.5 photocathode is increased as a consequence of the introduction of the Co_2P layer. Nevertheless, R_{ct} of the SiNW@Co_2P-4.5 electrode is significantly reduced, only amounting to 10.3 Ω, *ca.* 150 times smaller than that of the bare SiNW photocathode (R_{ct} = 1583 Ω, **Table S2**). This indicates that the deposited Co_2P catalyst layer has substantially expedited the charge transfer kinetics of SiNWs during solar-driven hydrogen evolution, which is consistent with the above M-S analysis.

Long-term stability under PEC operation conditions is of essential importance for practical deployment of PEC devices for solar-driven hydrogen production. Without appropriate passivation, Si-based photocathodes will be photo-oxidized in short period of time even in a strong acidic (i.e. reductant) solution, leading to the failure of devices [31, 44]. Presently, the most commonly used passivation strategy is to coat Si-based photoelectrodes with a continuous layer of

wide-band-gap semiconductor (e.g. TiO_2, SiO_2) that not only allows for the penetration of incident light but also has excellent chemical stability and enables tunneling for the transport of photo-generated charge carriers [37, 50, 51]. Recently, some researchers demonstrated that a continuous layer of HER catalysts having good enough electrochemical stability can effectively protect Si from oxidation [8, 20], besides helping to promote the HER, thus offering dual functions. Co_2P has been widely reported to have good electrochemical stability when used as an HER catalyst [46], and is therefore a good candidate of choice. **Figure 5d** shows the chronoamperometric curves of SiNW@Co_2P-4.5 mM and SiNW@Pt photocathodes recorded at 0 V *vs* RHE under 100 mW cm^{-2} illumination in 0.5 H_2SO_4. The photocurrent density of the SiNW@Co_2P photocathode slowly decreases in the beginning 3 hours and then gets stabilized at 17.9 mA cm^{-2} up to 20 hours without obvious degradation, exhibiting superior operational stability. The H_2 bubbles were evolving during the whole long-term stability test, as shown in the digital photograph in **Figure 5d** inset (see also **Movie S1**). In stark contrast, the photocurrent density of the SiNW@Pt photocathode diminishes quickly from the initial -14.2 mA cm^{-2} to -9.2 mA cm^{-2} within only 1 hour. In fact, Pt, despite its high activity for HER, has been proven to have poor electrochemical stability in harsh acidic or alkaline solutions due to the high mobility of Pt atoms under electrochemical conditions [52]. **Figure 5d** unambiguously demonstrates that the deposited conformal and continuous layer of Co_2P over SiNWs can indeed serve as a passivation layer, substantially improving the lifetime of photoelectrodes.

3. Conclusions

We have fabricated SiNW@Co_2P core/shell nanostructured photocathodes based on simple and cost-effective drop-casting of precursor solution on lithography-patterned Si nanowire arrays,

followed by a post-phosphorization treatment at an elevated temperature. The deposited Co_2P is conformal and continuous, and can serve both as a passivation layer to protect Si from photo-oxidation and as a catalyst layer to promote the hydrogen evolution reaction, showing favorable bi-functionality. Upon optimizing the drop-casting conditions, the best-performing SiNW@Co_2P photocathode exhibits a hydrogen evolution onset potential of +0.25 V *vs* RHE, a photocurrent density as high as -21.9 mA cm^{-2} at 0 V *vs* RHE and an excellent catalytic stability of 20 hours under photoelectrochemical hydrogen evolution conditions, outperforming many nanostructured Si photocathodes reported in the literature. Combining passivation and catalytic functions in a single continuous layer represents a promising strategy for designing high-performance photoelectrodes, which may simplify the fabrication procedures and potentially reduce the production cost. It can be expected that the photoelectrochemical hydrogen evolution performance would be further improved if Si nanowire electrodes with buried p-n junctions are used and coupled with a continuous layer of catalytically active and electrochemically stable HER catalysts.

4. Experimental Section

4.1 Fabrication of highly-ordered SiNW arrays:

The SiNW arrays were fabricated using e-beam lithography followed by deep reactive ion etching of Si. Briefly, a 200 nm thick AlCuSi film was sputter-coated (Singulus Timaris FTM) on the unpolished side of a p-type Si (100) wafer (Boron doped, 1–30 Ω cm, LG Silitron). A layer of 300 nm SiO_2 was then deposited on the polished surface of the Si wafer by plasma-enhanced chemical vapor deposition (PECVD, STPS MPX CVD). Subsequently, a layer of negative photoresist (ARN 7520, 200 nm) was spin-coated over the deposited SiO_2. Well-ordered arrays (7 mm × 7 mm) with a square pillar size of 150 nm and a pitch of 225 nm (center to center spacing)

were patterned by e-beam lithography (Vistec EBPG 5200) over the whole wafer. The pattern was developed and transferred into the underlying SiO_2 layer by reactive ion etching (RIE, SPTS APS ICP) to form a SiO_2 mesh mask for the subsequent deep RIE process (DRIE, SPTS Pegasus IDP) to obtain SiNW arrays of 1 μm length. A cleaning process was then followed using oxygen plasma (PVA TEPLA Plasma Asher) for 15 min. Afterwards, the SiO_2 layer on the top of the SiNWs was removed using HF vapor etcher (SPTS uEtch System). The Si wafer was diced into 12 mm × 20 mm pieces using a dicing saw (DISCO DAD 3350), with the patterned area (7 mm × 7 mm) in the center of each piece. The ohmic contact between AlCuSi and Si wafer was made by thermally annealing the as-diced pieces at 400 ^oC in high-purity nitrogen (N_2, 99.999%) for 1 min at a ramping rate of 2 $^oC\ min^{-1}$.

4.2 Fabrication of SiNW@Co_2P and SiNW@Pt:

The drop-casting technique was used to deposit Co precursors onto SiNWs. The drop-casting solution contained varying concentrations of $(CH_3COO)_2Co \cdot 4H_2O$ (Sigma-Aldrich) in ethanol (Sigma-Aldrich). The solution was stirred for 15 – 20 min until a clear pink solution was obtained. The solution was then drop-cast over the patterned SiNW electrode using micro-pipette (20 μL), and the Si photoelectrode was subsequently left in fume hood for slow evaporation of ethanol. The process of phosphorization was carried out in a tube furnace using red phosphorus (P, Sigma Aldrich) as the phosphorus source. The Si substrate was placed in a ceramic boat with 0.5 g of red P placed at the upstream side. The furnace was ramped to 500 ^oC at a rate of 10 $^oC\ min^{-1}$, kept at this temperature for 2 h, and then cooled down naturally to room temperature. A constant N_2 flow of 800 sccm passed through the work tube in the whole process. Pt decorated SiNW photocathodes (SiNW@Pt) were fabricated employing electroless deposition of Pt on

SiNWs under calibrated 1 sun conditions in a mixture of 0.001 M K_2PtCl_6 in 1 : 50 (H_2O : HF) of HF (48% HF Sigma Aldrich) solution for 1 min.

4.3 Characterization:

The morphology and microstructure of the samples were examined by scanning electron microscopy (SEM, FEI Quanta FEG 650) and aberration-corrected transmission electron microscopy (FEI Titan ChemiSTEM operating at 200 keV). For the TEM observations, the wires were scratched off the Si substrate and directly dispersed on a lacey carbon copper grid using water as a medium. The grid was then dried at 80°C in a vacuum oven.

4.4 Photoelectrochemical tests:

The PEC performance of the SiNW@Co_2P electrodes was evaluated in a three-electrode configuration with a graphite rod as the counter electrode and a saturated calomel electrode (SCE) as the reference. The electrolyte consisted of 0.5 M H_2SO_4 (Sigma-Aldrich) having a pH value of 0.3. The PEC tests were carried out in a jacketed quartz cell having a round flat window of quartz. A calibrated 1 sun solar simulator with a built-in AM 1.5 filter (Oriel® LCS-100^{TM}) was used as the light source. Linear scan voltammetry (LSV), electrochemical impedance spectroscopy (EIS), Mott-Schottky (M-S) analysis and chronoamperometry were performed using a Zennium electrochemical workstation (Zahner). The EIS measurements were conducted in the frequency range of 10 mHz – 200 kHz at a fixed potential of +0.15 V *vs* RHE under nominal illumination of 100 mW cm^{-2}, with an AC voltage amplitude of 10 mV. The sample temperature was maintained at 23 ^{o}C by circulating water through the water jacket of the PEC cell during the test using a refrigerated chiller (HAAKE Phoenix II, Thermo Scientific). Unless otherwise stated, all potentials are reported versus reversible hydrogen electrode (RHE) by converting the potentials measured versus SCE through the following equation:

$$\boldsymbol{U}_{(RHE)} = \boldsymbol{U}_{(SCE)} + 0.241 + 0.059 \times pH \qquad (3)$$

Acknowledgements

This work was funded by ERDF funds through the Portuguese Operational Programme for Competitiveness and Internationalization COMPETE 2020, and national funds through FCT – The Portuguese Foundation for Science and Technology, under the project "PTDC/CTM-ENE/2349/2014" (Grant Agreement No. 016660). The work is also partially funded by the Portugal-China Bilateral Collaborative Programme (FCT/21102/28/12/2016/S). L. F. Liu acknowledges the financial support of the FCT Investigator Grant (IF/01595/2014) and Exploratory Grant (IF/01595/2014/CP1247/CT0001). L. Qiao acknowledges the financial support of the Ministry of Science and Technology of China (Grant Agreement No. 2016YFE0132400).

References:

[1] Dincer, I. Renewable energy and sustainable development: a crucial review. *Renew Sust Energ Rev* **2000**, *4*, 157-175.

[2] Walter, M. G.;Warren, E. L.;McKone, J. R.;Boettcher, S. W.;Mi, Q. X.;Santori, E. A.; Lewis, N. S. Solar Water Splitting Cells. *Chem Rev* **2010**, *110*, 6446-6473.

[3] Cook, T. R.;Dogutan, D. K.;Reece, S. Y.;Surendranath, Y.;Teets, T. S.; Nocera, D. G. Solar Energy Supply and Storage for the Legacy and Non legacy Worlds. *Chem Rev* **2010**, *110*, 6474-6502.

[4] Lewis, N. S.; Nocera, D. G. Powering the planet: Chemical challenges in solar energy utilization. *P Natl Acad Sci USA* **2006**, *103*, 15729-15735.

[5] Reece, S. Y.;Hamel, J. A.;Sung, K.;Jarvi, T. D.;Esswein, A. J.;Pijpers, J. J. H.; Nocera, D. G. Wireless Solar Water Splitting Using Silicon-Based Semiconductors and Earth-Abundant Catalysts. *Science* **2011**, *334*, 645-648.

[6] Sun, K.;Shen, S. H.;Liang, Y. Q.;Burrows, P. E.;Mao, S. S.; Wang, D. L. Enabling Silicon for Solar-Fuel Production. *Chem Rev* **2014**, *114*, 8662-8719.

[7] Candea, R. M.;Kastner, M.;Goodman, R.; Hickok, N. Photoelectrolysis of Water - Si in Salt-Water. *J Appl Phys* **1976**, *47*, 2724-2726.

[8] Bao, X. Q.;Petrovykh, D. Y.;Alpuim, P.;Stroppa, D. G.;Guldris, N.;Fonseca, H.;Costa, M.;Gaspar, J.;Jin, C. H.; Liu, L. F. Amorphous oxygen-rich molybdenum oxysulfide Decorated p-type silicon microwire Arrays for efficient photoelectrochemical water reduction. *Nano Energy* **2015**, *16*, 130-142.

[9] Yuhas, B. D.;Smeigh, A. L.;Samuel, A. P. S.;Shim, Y.;Bag, S.;Douvalis, A. P.;Wasielewski, M. R.; Kanatzidis, M. G. Biomimetic Multifunctional Porous Chalcogels as Solar Fuel Catalysts. *J Am Chem Soc* **2011**, *133*, 7252-7255.

[10] Li, W.;Wang, X. G.;Xiong, D. H.; Liu, L. F. Efficient and durable electrochemical hydrogen evolution using cocoon-like MoS2 with preferentially exposed edges. *Int J Hydrogen Energ* **2016**, *41*, 9344-9354.

[11] Gholamvand, Z.;McAteer, D.;Backes, C.;McEvoy, N.;Harvey, A.;Berner, N. C.;Hanlon, D.;Bradley, C.;Godwin, I.;Rovetta, A.;Lyons, M. E. G.;Duesberg, G. S.; Coleman, J. N. Comparison of liquid exfoliated transition metal dichalcogenides reveals MoSe2 to be the most effective hydrogen evolution catalyst. *Nanoscale* **2016**, *8*, 5737-5749.

[12] Zhang, L. M.;Liu, C.;Wong, A. B.;Resasco, J.; Yang, P. D. MoS2-wrapped silicon nanowires for photoelectrochemical water reduction. *Nano Res* **2015**, *8*, 281-287.

[13] Xiong, D. H.;Zhang, Q. Q.;Thalluri, S. M.;Xu, J. Y.;Li, W.;Fu, X. L.; Liu, L. F. One-Step Fabrication of Monolithic Electrodes Comprising Co9S8 Particles Supported on Cobalt Foam for Efficient and Durable Oxygen Evolution Reaction. *Chem-Eur J* **2017**, *23*, 8749-8755.

[14] Chen, C. J.;Yang, K. C.;Basu, M.;Lu, T. H.;Lu, Y. R.;Dong, C. L.;Hu, S. F.; Liu, R. S. Wide Range pH-Tolerable Silicon@Pyrite Cobalt Dichalcogenide Microwire Array Photoelectrodes for Solar Hydrogen Evolution. *Acs Appl Mater Inter* **2016**, *8*, 5400-5407.

[15] Li, W.;Gao, X. F.;Xiong, D. H.;Wei, F.;Song, W. G.;Xu, J. Y.; Liu, L. F. Hydrothermal Synthesis of Monolithic Co3Se4 Nanowire Electrodes for Oxygen Evolution and Overall Water Splitting with High Efficiency and Extraordinary Catalytic Stability. *Adv Energy Mater* **2017**, *7*, 7.

[16] Popczun, E. J.;McKone, J. R.;Read, C. G.;Biacchi, A. J.;Wiltrout, A. M.;Lewis, N. S.; Schaak, R. E. Nanostructured Nickel Phosphide as an Electrocatalyst for the Hydrogen Evolution Reaction. *J Am Chem Soc* **2013**, *135*, 9267-9270.

[17] Wang, X. G.;Kolen'ko, Y. V.;Bao, X. Q.;Kovnir, K.; Liu, L. F. One-Step Synthesis of Self-Supported Nickel Phosphide Nanosheet Array Cathodes for Efficient Electrocatalytic Hydrogen Generation. *Angew Chem Int Edit* **2015**, *54*, 8188-8192.

[18] Roske, C. W.;Popczun, E. J.;Seger, B.;Read, C. G.;Pedersen, T.;Hansen, O.;Vesborg, P. C. K.;Brunschwig, B. S.;Schaak, R. E.;Chorkendorff, I.;Gray, H. B.; Lewis, N. S. Comparison of the Performance of CoP-Coated and Pt-Coated Radial Junction n(+)p-Silicon Microwire-Array Photocathodes for the Sunlight-Driven Reduction of Water to H-2(g). *J Phys Chem Lett* **2015**, *6*, 1679-1683.

[19] Bao, X. Q.;Cerqueira, M. F.;Alpuim, P.; Liu, L. F. Silicon nanowire arrays coupled with cobalt phosphide spheres as low-cost photocathodes for efficient solar hydrogen evolution. *Chem Commun* **2015**, *51*, 10742-10745.

[20] Hellstern, T. R.;Benck, J. D.;Kibsgaard, J.;Hahn, C.; Jaramillo, T. F. Engineering Cobalt Phosphide (CoP) Thin Film Catalysts for Enhanced Hydrogen Evolution Activity on Silicon Photocathodes. *Adv Energy Mater* **2016**, *6*.

[21] Wang, X. G.;Li, W.;Xiong, D. H.;Petrovykh, D. Y.; Liu, L. F. Bifunctional Nickel Phosphide Nanocatalysts Supported on Carbon Fiber Paper for Highly Effi cient and Stable Overall Water Splitting. *Adv Funct Mater* **2016**, *26*, 4067-4077.

[22] Li, W.;Gao, X. F.;Wang, X. G.;Xiong, D. H.;Huang, P. P.;Song, W. G.;Bao, X. Q.; Liu, L. F. From water reduction to oxidation: Janus Co-Ni-P nanowires as high-efficiency and

ultrastable electrocatalysts for over 3000 h water splitting. *J Power Sources* **2016**, *330*, 156-166.

[23] Li, W.;Gao, X. F.;Xiong, D. H.;Xia, F.;Liu, J.;Song, W. G.;Xu, J. Y.;Thalluri, S. M.;Cerqueira, M. F.;Fu, X. L.; Liu, L. F. Vapor-solid synthesis of monolithic single-crystalline CoP nanowire electrodes for efficient and robust water electrolysis. *Chem Sci* **2017**, *8*, 2952-2958.

[24] Li, W.;Xiong, D. H.;Gao, X. F.;Song, W. G.;Xia, F.; Liu, L. F. Self-supported Co-Ni-P ternary nanowire electrodes for highly efficient and stable electrocatalytic hydrogen evolution in acidic solution. *Catal Today* **2017**, *287*, 122-129.

[25] Wu, H. B.;Xia, B. Y.;Yu, L.;Yu, X. Y.; Lou, X. W. Porous molybdenum carbide nano-octahedrons synthesized via confined carburization in metal-organic frameworks for efficient hydrogen production. *Nat Commun* **2015**, *6*.

[26] Ma, B. J.;Xu, H. J.;Lin, K. Y.;Li, J.;Zhan, H. J.;Liu, W. Y.; Li, C. Mo2C as Non-Noble Metal Co-Catalyst in Mo2C/CdS Composite for Enhanced Photocatalytic H-2 Evolution under Visible Light Irradiation. *Chemsuschem* **2016**, *9*, 820-824.

[27] Gong, Q. F.;Wang, Y.;Hu, Q.;Zhou, J. G.;Feng, R. F.;Duchesne, P. N.;Zhang, P.;Chen, F. J.;Han, N.;Li, Y. F.;Jin, C. H.;Li, Y. G.; Lee, S. T. Ultrasmall and phase-pure W2C nanoparticles for efficient electrocatalytic and photoelectrochemical hydrogen evolution. *Nat Commun* **2016**, *7*.

[28] Yang, Y.;Wang, M.;Zhang, P. L.;Wang, W. H.;Han, H. X.; Sunt, L. C. Evident Enhancement of Photoelectrochemical Hydrogen Production by Electroless Deposition of M-B (M = Ni, Co) Catalysts on Silicon Nanowire Arrays. *Acs Appl Mater Inter* **2016**, *8*, 30143-30151.

[29] Vrubel, H.; Hu, X. L. Molybdenum Boride and Carbide Catalyze Hydrogen Evolution in both Acidic and Basic Solutions. *Angew Chem Int Edit* **2012**, *51*, 12703-12706.

[30] Shalom, M.;Ressnig, D.;Yang, X. F.;Clavel, G.;Fellinger, T. P.; Antonietti, M. Nickel nitride as an efficient electrocatalyst for water splitting. *J Mater Chem A* **2015**, *3*, 8171-8177.

[31] Bae, D.;Seger, B.;Vesborg, P. C. K.;Hansen, O.; Chorkendorff, I. Strategies for stable water splitting via protected photoelectrodes. *Chem Soc Rev* **2017**, *46*, 1933-1954.

[32] Chandrasekaran, S.;Nann, T.; Voelcker, N. H. Nanostructured silicon photoelectrodes for solar water electrolysis. *Nano Energy* **2015**, *17*, 308-322.

[33] Dalchiele, E. A.;Martin, F.;Leinen, D.;Marotti, R. E.; Ramos-Barrado, J. R. Single-Crystalline Silicon Nanowire Array-Based Photoelectrochemical Cells. *J Electrochem Soc* **2009**, *156*, K77-K81.

[34] Jung, J. Y.;Choi, M. J.;Zhou, K.;Li, X. P.;Jee, S. W.;Um, H. D.;Park, M. J.;Park, K. T.;Bang, J. H.; Lee, J. H. Photoelectrochemical water splitting employing a tapered silicon nanohole array. *J Mater Chem A* **2014**, *2*, 833-842.

[35] Zhang, B. C.;Wang, H.;He, L.;Duan, C. Y.;Li, F.;Ou, X. M.;Sun, B. Q.; Zhang, X. H. The diameter-dependent photoelectrochemical performance of silicon nanowires. *Chem Commun* **2016**, *52*, 1369-1372.

[36] Sim, U.;Jeong, H. Y.;Yang, T. Y.; Nam, K. T. Nanostructural dependence of hydrogen production in silicon photocathodes. *J Mater Chem A* **2013**, *1*, 5414-5422.

[37] Bazri, B.;Lin, Y. C.;Lu, T. H.;Chen, C. J.;Kowsari, E.;Hu, S. F.; Liu, R. S. A heteroelectrode structure for solar water splitting: integrated cobalt ditelluride across a TiO2-passivated silicon microwire array. *Catal Sci Technol* **2017**, *7*, 1488-1496.

[38] Choi, S. K.;Piao, G.;Choi, W.; Park, H. Highly efficient hydrogen production using p-Si wire arrays and NiMoZn heterojunction photocathodes. *Appl Catal B-Environ* **2017**, *217*, 615-621.

[39] Huang, Z. P.;Wang, C. F.;Pan, L.;Tian, F.;Zhang, X. X.; Zhang, C. Enhanced photoelectrochemical hydrogen production using silicon nanowires@MoS3. *Nano Energy* **2013**, *2*, 1337-1346.

[40] Basu, M.;Zhang, Z. W.;Chen, C. J.;Chen, P. T.;Yang, K. C.;Ma, C. G.;Lin, C. C.;Hu, S. F.; Liu, R. S. Heterostructure of Si and CoSe2: A Promising Photocathode Based on a Non-noble Metal Catalyst for Photoelectrochemical Hydrogen Evolution. *Angew Chem Int Edit* **2015**, *54*, 6211-6216.

[41] Seger, B.;Pedersen, T.;Laursen, A. B.;Vesborg, P. C. K.;Hansen, O.; Chorkendorff, I. Using TiO2 as a Conductive Protective Layer for Photocathodic H-2 Evolution. *J Am Chem Soc* **2013**, *135*, 1057-1064.

[42] Seger, B.;Laursen, A. B.;Vesborg, P. C. K.;Pedersen, T.;Hansen, O.;Dahl, S.; Chorkendorff, I. Hydrogen Production Using a Molybdenum Sulfide Catalyst on a Titanium-Protected n plus p-Silicon Photocathode. *Angew Chem Int Edit* **2012**, *51*, 9128-9131.

[43] Bae, D.;Shayestehaminzadeh, S.;Thorsteinsson, E. B.;Pedersen, T.;Hansen, O.;Seger, B.;Vesborg, P. C. K.;Olafsson, S.; Chorkendorff, I. Protection of Si photocathode using TiO2 deposited by high power impulse magnetron sputtering for H-2 evolution in alkaline media. *Sol Energ Mat Sol C* **2016**, *144*, 758-765.

[44] Bao, X. Q.; Liu, L. F. Improved photo-stability of silicon nanobelt arrays by atomic layer deposition for efficient photocatalytic hydrogen evolution. *J Power Sources* **2014**, *268*, 677-682.

[45] Tian, J. Q.;Liu, Q.;Asiri, A. M.; Sun, X. P. Self-Supported Nanoporous Cobalt Phosphide Nanowire Arrays: An Efficient 3D Hydrogen-Evolving Cathode over the Wide Range of pH 0-14. *J Am Chem Soc* **2014**, *136*, 7587-7590.

[46] Callejas, J. F.;Read, C. G.;Popczun, E. J.;McEnaney, J. M.; Schaak, R. E. Nanostructured Co2P Electrocatalyst for the Hydrogen Evolution Reaction and Direct Comparison with Morphologically Equivalent CoP. *Chem Mater* **2015**, *27*, 3769-3774.

[47] Choi, S. K.;Chae, W. S.;Song, B.;Cho, C. H.;Choi, J.;Han, D. S.;Choi, W.; Park, H. Photoelectrochemical hydrogen production on silicon microwire arrays overlaid with ultrathin titanium nitride. *J Mater Chem A* **2016**, *4*, 14008-14016.

[48] Huang, Z. P.;Zhong, P.;Wang, C. F.;Zhang, X. X.; Zhang, C. Silicon Nanowires/Reduced Graphene Oxide Composites for Enhanced Photoelectrochemical Properties. *Acs Appl Mater Inter* **2013**, *5*, 1961-1966.

[49] Sim, U.;Moon, J.;An, J.;Kang, J. H.;Jerng, S. E.;Moon, J.;Cho, S. P.;Hong, B. H.; Nam, K. T. N-doped graphene quantum sheets on silicon nanowire photocathodes for hydrogen production. *Energ Environ Sci* **2015**, *8*, 1329-1338.

[50] Esposito, D. V.;Levin, I.;Moffat, T. P.; Talin, A. A. H-2 evolution at Si-based metal-insulator-semiconductor photoelectrodes enhanced by inversion channel charge collection and H spillover. *Nat Mater* **2013**, *12*, 562-568.

[51] Hu, S.;Shaner, M. R.;Beardslee, J. A.;Lichterman, M.;Brunschwig, B. S.; Lewis, N. S. Amorphous TiO2 coatings stabilize Si, GaAs, and GaP photoanodes for efficient water oxidation. *Science* **2014**, *344*, 1005-1009.

[52] Erlebacher, J. An atomistic description of dealloying - Porosity evolution, the critical potential, and rate-limiting behavior. *J Electrochem Soc* **2004**, *151*, C614-C626.

Figure Captions

Figure 1. Schematic illustration of the fabrication of SiNW@Co_2P photocathodes.

Figure 2. SEM images showing the morphology of (a) as-fabricated SiNW arrays and SiNW@Co_2P photocathodes prepared with cobalt precursor concentrations of (b) 9 mM, (c) 18 mM and (d) 36 mM.

Figure 3. (a) Montage TEM image showing conformal and continuous deposition of the Co_2P layer on SiNW. (b) EDS signal map showing the distribution of Co_2P along the SiNW. The intensity of Co_2P is more predominant around the root than that on the top. (c, d) High-magnification TEM images of SiNW@Co_2P. Inset of (d): SAED pattern taken over the Co_2P nanoparticles. (e) HRTEM image.

Figure 4. (a) HAADF-STEM image of an individual SiNW@Co_2P and the elemental maps of (b) Si, (c) Co, (d) P and (e) their overlay.

Figure 5. (a) Linear scan voltammograms of bare SiNW, SiNW@Pt and SiNW@Co_2P photocathodes recorded under 100 mW cm^{-2} illumination. (b) Mott-Schottky plots of bare SiNW and SiNW@Co_2P-4.5 photocathodes measured in the dark at 10 kHz. (c) Nyquist plots of the bare SiNW and SiNW@Co_2P-4.5 photocathodes recorded at +0.15 V *vs* RHE under 100 mW cm^{-2} illumination. Insets: zoomed view in the high frequency region (left) and equivalent circuit models (right). (d) Long-term stability tests conducted at 0 V *vs* RHE for SiNW@Pt and SiNW@Co_2P-

4.5 photocathodes. All the measurements were carried out in 0.5 M H_2SO_4 solution at room temperature.

Figures

Figure 1. Thalluri et al.

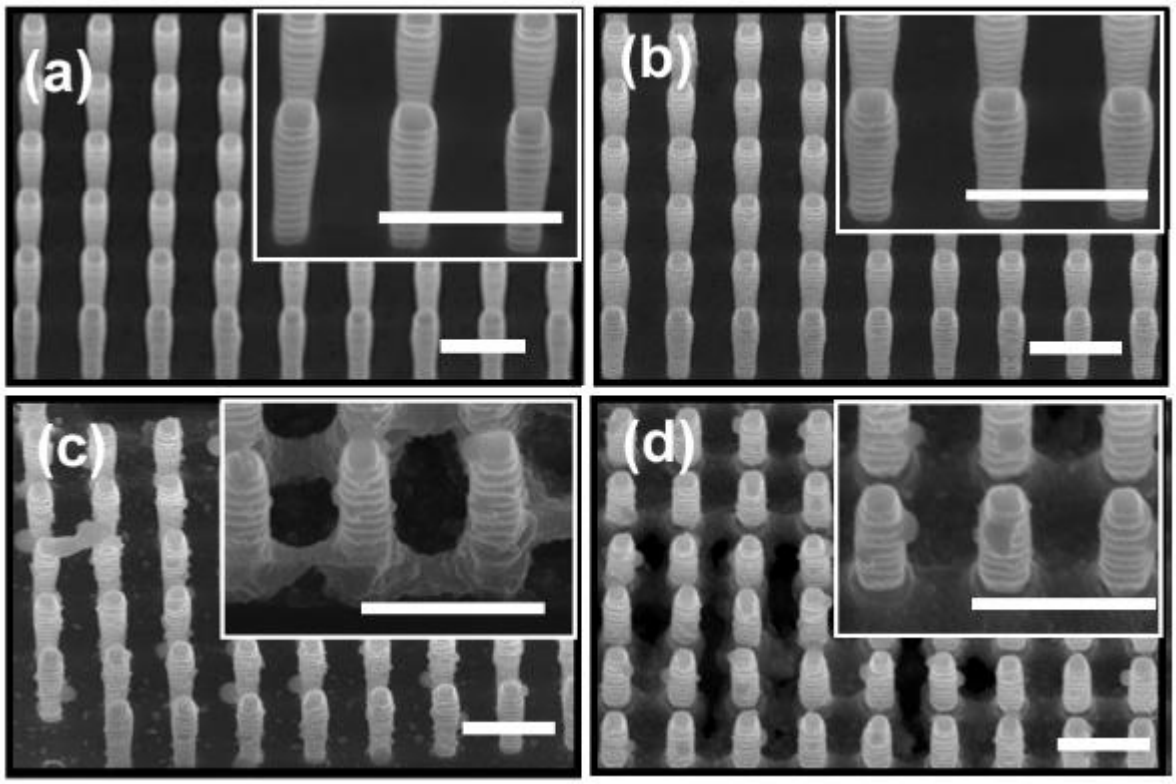

Figure 2. Thalluri et al.

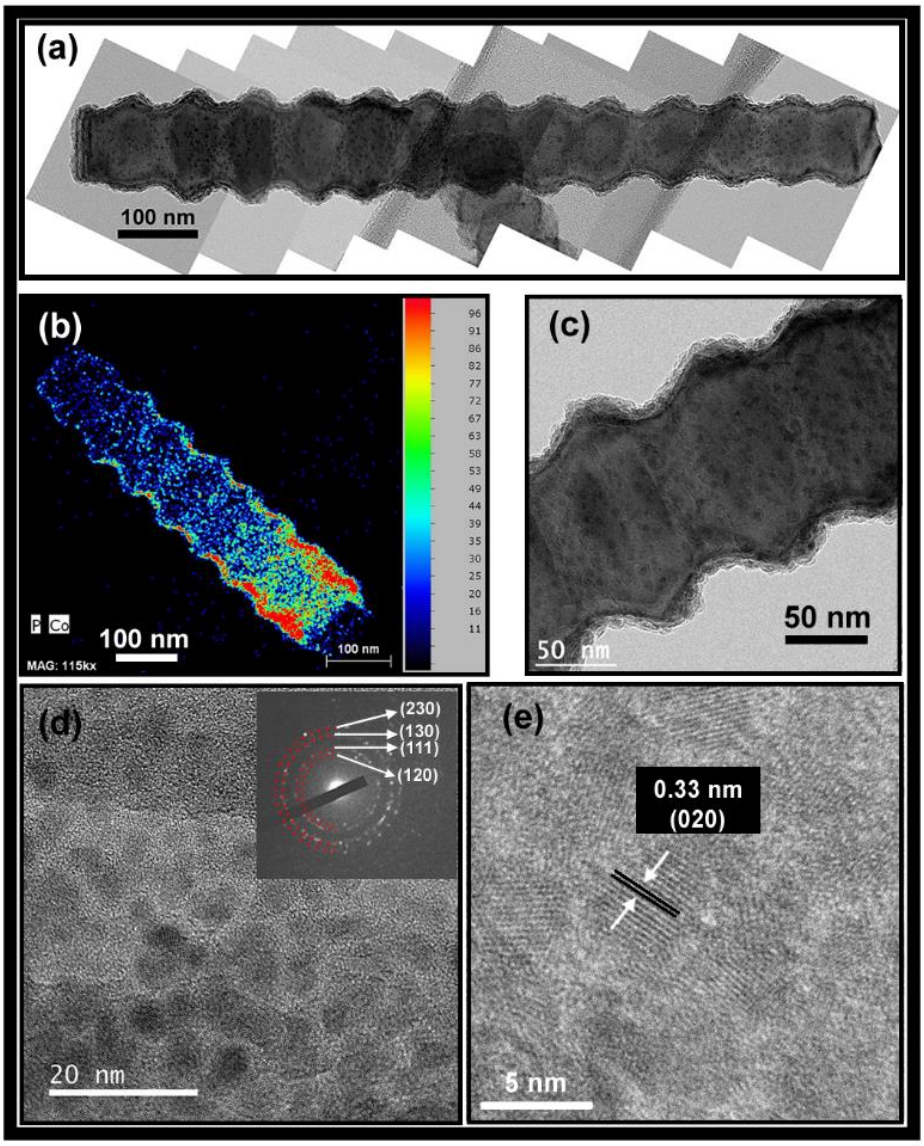

Figure 3. Thalluri et al.

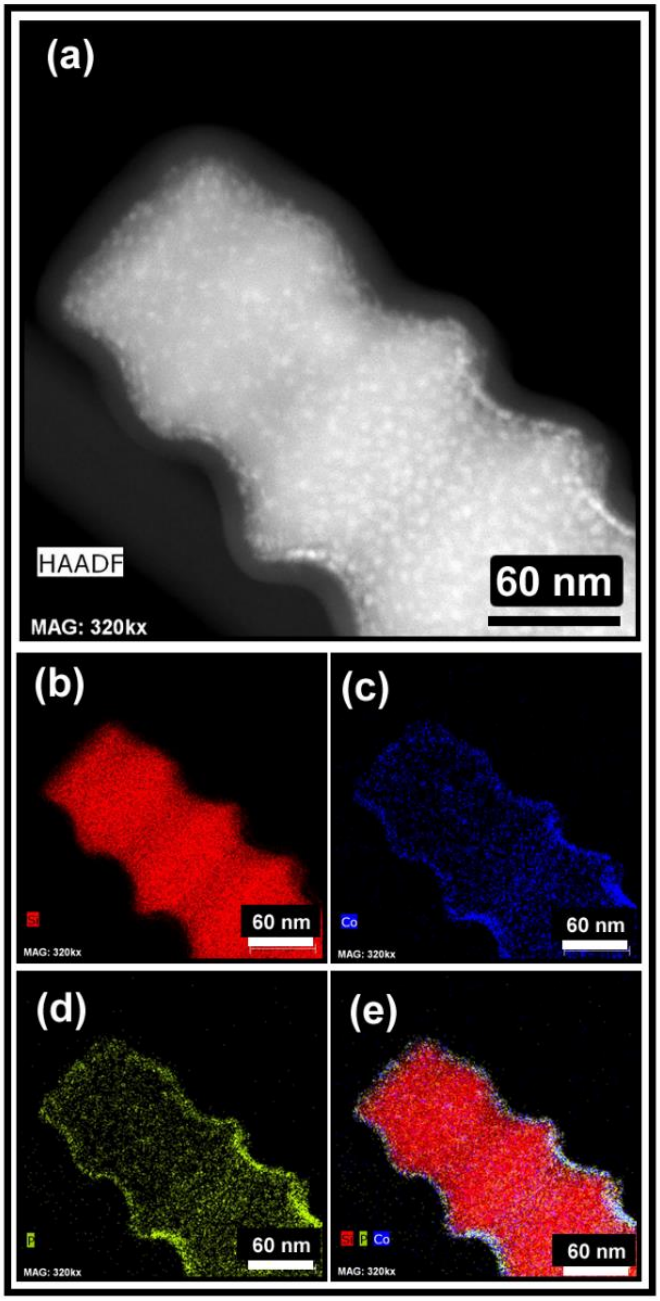

Figure 4. Thalluri et al.

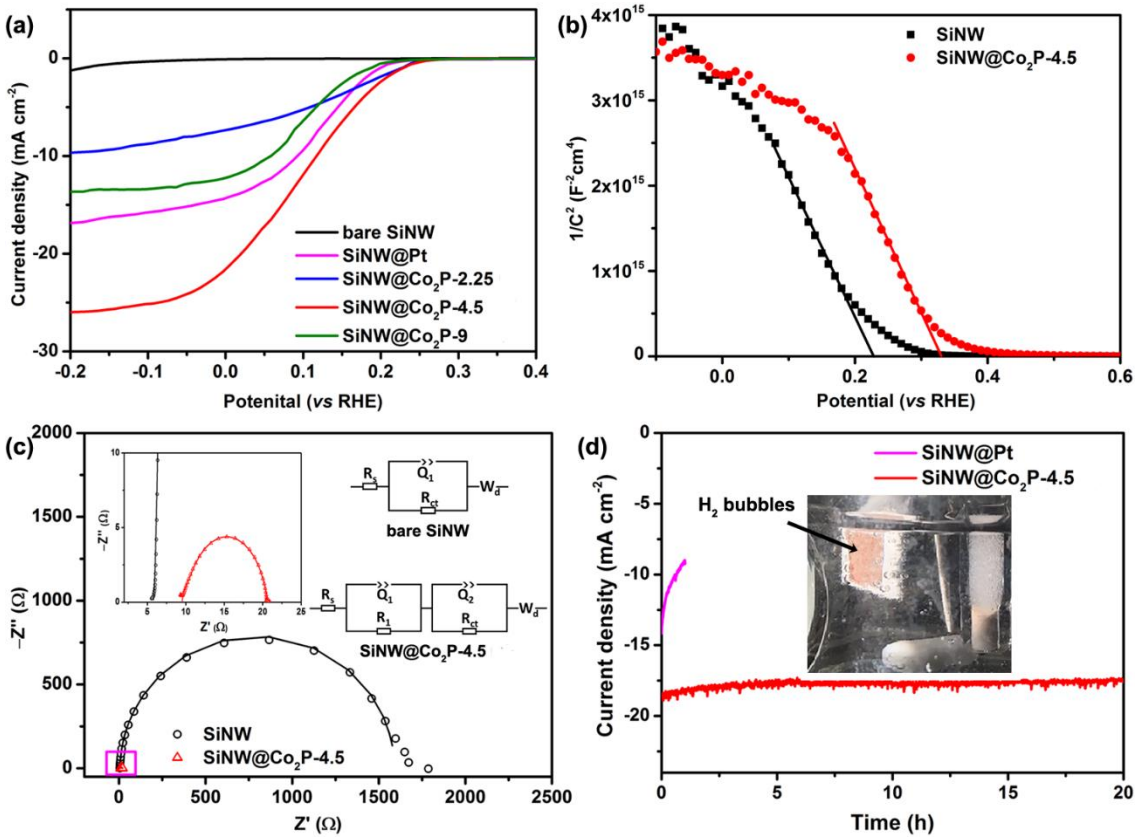

Figure 5. Thalluri et al.